Time Transition of Activated Conductivity Distribution in Air and Charge Accumulation in Air-solid Composite Insulation Systems under DC Partial Discharge

Ryuichi Nakane, Hiroki Kojima and **Naoki Hayakawa**
Department of Electrical Engineering, Nagoya University
Furo-cho, Chikusa-ku, Nagoya 464-8603, Japan

ABSTRACT

In this study, charge behavior in gas and on solid insulator due to DC partial discharge (DC-PD) is investigated by using needle-air-PMMA-plane electrode configuration under negative DC voltage. The time evolution of surface potential distributions on solid insulator is measured and compared with the simulation results taking into account the charge behavior in air, such as generation, recombination and motion of positive and negative ions. Especially, a novel transport equation model considering the source of charge carrier due to DC-PD is built. Consequently, in air-solid composite insulation systems under negative DC voltage application, the time transition of activated conductivity distribution in air by DC-PD contributing to the charge accumulation on PMMA surface is evaluated quantitatively. The activated conductivity in air is distributed in the range from 1.0×10^{-9} to 3.0×10^{-9} S/m under DC-PD, which is approximately 10^{10} times higher than that in non-activated conductivity space by natural ionization. In addition, the activated conductivity distribution in air dominantly contributes to the charge accumulation process from initial state (DC-on) to DC steady-state. The activated conductivity is the crucial parameter for DC electrical insulation in case that charge behavior is activated in gas medium under DC-PD.

Index Terms — **HVDC, air-solid composite insulation, charge accumulation, partial discharge, electric field, conductivity in air**

1 INTRODUCTION

HIGH voltage direct current (HVDC) transmission technologies have been utilized worldwide in numerous power systems for such as long distance overhead lines and interconnecting two AC networks of different frequencies [1]. Therefore, it is necessary to enhance DC electrical insulation performance of DC power apparatus from the view point of reliability.

In DC power equipments, however, DC electrical insulation exhibits a lot of complicated features that differ from conventional AC electrical insulation [2, 3]. As one of the main factors for the reduction of electrical insulation performance in DC power apparatus such as DC gas insulated switchgear (DC-GIS) and DC gas insulated transmission line (DC-GIL), the charge accumulation on solid insulator to support high voltage conductor is considered. The distorted electric field distribution by charge accumulation may lead to the reduction of DC electrical insulation performance under polarity reversal and the impulse superimposed voltage [3, 4]. It is required to concentrate researches on a better understanding of unique behavior such as DC partial discharge (DC-PD), charging accumulation on solid insulator surface and DC electric field distribution in gas-solid composite insulation systems [5-7].

When charge accumulation phenomena are discussed in gas-solid DC composite insulation such as DC-GIS, it is important to clearly identify the main source of charge carrier. This is because the electric conductivity that determines DC electric field distribution significantly depends on the state of the source of charge carrier. In addition, the experimental and analytical approaches for investigating charging processes are also different depending on the source of charge carrier. Generally, in actual GIS structure, natural ionization by cosmic ray and charge injection from electrode to solid insulator are expected as the main source of charge carrier under normal conditions [8, 9]. In this situation, a low equivalent conductivity mainly depending on the natural ionization due to cosmic ray is distributed in gas. Some authors call this the “capture volume” [8, 10], others “active gas volume” [7]. If the charge carriers are generated by natural radiation, the surface charge accumulation is dominated by the gas volume that is connected to the surface via the electric line of force between electrode and solid insulator.

On the other hand, in the case of abnormal conditions where significant or irregular charge accumulation emerges, PD from

Manuscript received on 1 October 2020, in final form XX Month xxxx, accepted ssss Month 20yy. Corresponding author: R. Nakane.

protrusions or field electron emission due to electrode surface roughness could be assumed [11-13]. In the case of charge accumulation on solid insulator through gas region due to PD, the significantly activated conductivity could emerge from the source of PD and be distributed in gas medium. It is easy to qualitatively predict that the remarkable charge accumulation on solid insulator would occur due to the significant source of charge carrier such as PD, however, the relationship between the activated conductivity distribution and the charge accumulation process on solid insulator has not yet been clarified quantitatively.

The purpose of this paper is to clarify the mechanism for the time transition of charge accumulation process on solid insulator due to DC-PD in gas-solid composite insulation system in terms of the activated conductivity distribution in gas. As fundamental gas and solid insulator, air and polymethyl methacrylate (PMMA) are used in this paper. A novel transport equation model considering the generation of charge carrier in air due to DC-PD has been built. The time transition of conductivity distribution in air corresponding to the charge accumulation on PMMA is estimated quantitatively under DC-PD.

2 EXPERIMENTAL SETUP AND SIMULATION METHOD

2.1 EXPERIMENTAL SETUP

Figure 1 shows the experimental setup in air-solid composite insulation system under negative DC voltage. Experiments were conducted using a stainless steel needle electrode (tip radius: 100 μm) and a grounded plane electrode with 30 mm gap. A PMMA plate (Φ150 mm, t5 mm) was used as a solid insulator on the plane electrode. PMMA surface was cleaned with ethanol before voltage application. Negative DC 10 kV (PDIV: -6.5 kV) was applied for 1 min until saturation of deposited charges (DC steady-state). In this paper, we investigated the charging process until DC-PD for charge supply was suppressed by charge accumulation. Negative charges were accumulated on PMMA due to DC PD at the needle tip. In this experiment, it was verified that the deposited charges saturated in approximately 2 s. The current pulse due to DC-PD was detected by a high frequency current transformer (CT) to discuss the frequency and charge amount of DC-PD. In addition, the light emission of DC-PD around the needle tip was observed by using a digital camera with an image intensifier to discuss the shape and size of DC-PD.

After DC voltage application for the pre-determined time and dropping the DC voltage to 0, the surface potential distribution on PMMA from initial state (DC-on) to DC steady-state was measured with the time interval of 5 seconds between the measuring points with a certain speed by using a surface potential meter with electrostatic capacitive probe and X-stage. All experiments were carried out under ambient room temperature (298 K), atmospheric pressure (0.1 MPa-abs) and 50-70 % relative humidity in air. Table 1 shows the dielectric properties of air and PMMA used in this paper. The calculation method of the volume conductivity in air is explained in the next section.

Table 1. Dielectric properties of air and PMMA

Parameter	Unit	Air	PMMA
Relative permittivity : ε_r	-	1	3.55 (1 kHz)
Volume conductivity : σ_v	[S/m]	$e \cdot (n^+\mu^+ + n^-\mu^-)$	10^{-17} (298 K)
Surface conductivity : σ_s	[S]	-	10^{-15} (298 K)

2.2 TIME TRANSITION ANALYSIS OF DC ELECTRIC FIELD DISTRIBUTION CONSIDERING CHARGE ACTIVITY IN AIR

In air-solid composite insulation under DC voltage, the electric field distribution is distorted by the charge accumulation and its time transition. Immediately after DC voltage application (DC-on), capacitive field depending on the permittivity of the insulating materials is formed. After a certain time, the electric field distribution transits to resistive field depending on the conductivity [14]. When the charging process is investigated in air-solid composite insulation, the charge carrier transport equations in air should be solved in consideration of the generation, recombination and motion of positive and negative ions. This is because the conductivity in air depends on the activity of charge carriers such as positive and negative ions. In addition, DC-PD at the needle tip can be the main source of charge carrier for charging phenomena in this paper. Therefore, the conductivity in air would be activated and determine the charge accumulation process on PMMA.

In this paper, the electric field distribution from DC-on to DC steady-state is calculated by solving the positive and negative ion continuity Equations (1) - (2) coupled with Poisson's Equation (3) for the electric potential φ as follows [15]:

$$\frac{\partial n^+}{\partial t} = N_0 - k_r n^+ n^- - \mathrm{div}(n^+ \mu^+ \boldsymbol{E}) + D^+ \nabla^2 n^+ \quad (1)$$

$$\frac{\partial n^-}{\partial x} = N_0 - k_r n^+ n^- + \mathrm{div}(n^- \mu^- \boldsymbol{E}) + D^- \nabla^2 n^- \quad (2)$$

$$\nabla^2 \varphi = -\frac{e \cdot (n^+ - n^-)}{\varepsilon_0 \varepsilon_r} \quad (3)$$

where N_0: ion pair generation rate, k_r: ion-ion recombination coefficient, n^+, n^-: positive and negative ion density, μ^+, μ^-: mobility of positive and negative ions, D^+, D^-: diffusion

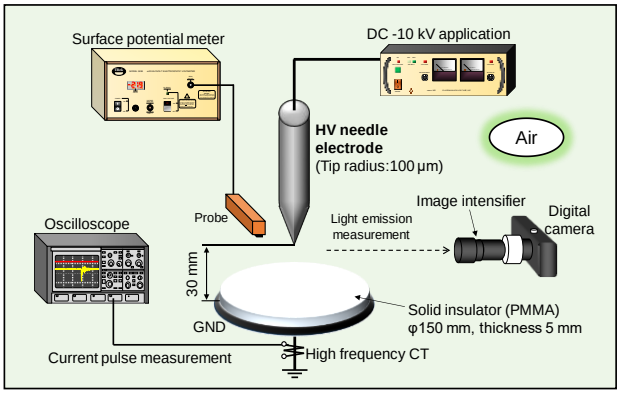

Figure 1. Experimental setup in air-solid composite insulation system under negative DC voltage.

coefficient of positive and negative ions, e: elementary charge, ε_0: permittivity of vacuum, ε_r: relative permittivity of insulating materials.

The conduction current density $\boldsymbol{J}_{\mathrm{Air}}$ in air considering drift and diffusion current, and $\boldsymbol{J}_{\mathrm{PMMA}}$ in PMMA can be described [14]:

$$\boldsymbol{J}_{\mathrm{Air}} = \mathrm{e}(n^+\mu^+ + n^-\mu^-)\boldsymbol{E} - \mathrm{e}\cdot\mathrm{grad}(D^+n^+ - D^-n^-) \quad (4)$$

$$\boldsymbol{J}_{\mathrm{PMMA}} = \sigma_{\mathrm{v\_PMMA}}\boldsymbol{E} \quad (5)$$

where $\sigma_{\mathrm{v\_PMMA}}$: volume conductivity in PMMA. The accumulated surface charge density q at the interface between air and PMMA from DC-on to DC steady-state is calculated based on the following Equation [15]:

$$\frac{\partial q}{\partial t} = \frac{\partial \varepsilon_{\mathrm{air}}\boldsymbol{E}_{\mathrm{Airn}}}{\partial t} - \frac{\partial \varepsilon_{\mathrm{PMMA}}\boldsymbol{D}_{\mathrm{PMMAn}}}{\partial t} = \boldsymbol{J}_{\mathrm{PMMAn}} - \boldsymbol{J}_{\mathrm{Airn}} - \mathrm{div}(\sigma_s \cdot E_t) \quad (6)$$

where $\boldsymbol{J}_{\mathrm{PMMAn}}$, $\boldsymbol{J}_{\mathrm{airn}}$: normal component of the conduction current density to insulator surface in PMMA and air, $\boldsymbol{E}_{\mathrm{PMMAn}}$, $\boldsymbol{E}_{\mathrm{airn}}$: normal component of the electric field to insulator surface in PMMA and air, $\varepsilon_{\mathrm{PMMA}}$, $\varepsilon_{\mathrm{air}}$: permittivity of PMMA and air, σ_s: surface conductivity, E_t: tangential component of the electric field on the insulator, q: surface charge density at the interface. These simulation parameters for positive and negative ions used in this paper are shown in Table 2 [15, 16].

The following condition was applied to initial values for positive and negative ion density in air at the time $t_0 = 0$ s [8].

$$n^+(t_0) = n^-(t_0) = \sqrt{\frac{N_0}{k_r}} \quad (7)$$

For boundary conditions, the simulation model with no charge injection into air is assumed. Therefore, the following boundary conditions (8) - (9) for positive ion were applied according to the normal component of electric field $\boldsymbol{E}_n$ to boundary [17].

$$n^+ = 0 \ (\boldsymbol{E}_n < 0) \quad (8)$$

$$\nabla n^+ = 0 \ (\boldsymbol{E}_n \geq 0) \quad (9)$$

In the case of negative ion, the following boundary conditions (10) - (11) were applied.

$$n^- = 0 \ (\boldsymbol{E}_n > 0) \quad (10)$$

$$\nabla n^- = 0 \ (\boldsymbol{E}_n \leq 0) \quad (11)$$

2.3 SIMULATION MODEL FOR CHARGE CARRIER GENERATION BY DC PARTIAL DISCHARGE

In the experiment, DC-PD at the needle tip can be the main source of charge carrier generation. The negative ions generated due to DC-PD drift in the direction of electric field and accumulate on PMMA surface under negative DC voltage. The magnitude and distribution of the accumulated charge on solid insulator are expected to be determined by the activated conductivity in air by DC-PD. Especially, the time transition of the conductivity distribution in air could be significantly affected by the state of DC-PD at the needle tip. In other words, it is required to consider DC-PD generation area at the needle tip to discuss the charge accumulation behavior in air-solid composite insulation in terms of the conductivity distribution in air. This means that the generation rate of negative ion at the needle tip by DC-PD should be applied to the simulation model. To derive the generation rate of negative ion, we experimentally measured the shape, that is, "DC-PD equivalent diameter", the frequency of DC-PD and the amount of charge.

Table 2. Simulation parameters for positive/negative ion.

Parameter	Unit	Positive ion	Negative ion
Ion pair generation rate : N_o	[1/(cm³ · s)]	10	
Recombination coefficient : k_r	[cm³/s]	2.2×10^{-6}	
Ion mobility : μ	[cm²/(V · s)]	1.36	1.87
Ion diffusion coefficient : D	[cm²/s]	3.51×10^{-2}	4.83×10^{-2}

Figure 2a shows the light emission of DC-PD at the needle tip with image intensifier. Note that the photograph in Figure 2a was taken by summing light emission for 2 s of negative DC voltage application. The light emission image reveals that a sphere-like luminous area appears at the needle tip. Assuming that the shape of the source of charge carrier at the needle tip is sphere, we estimated the generation rate of negative ion with the following equation:

$$N_{\mathrm{ion}} = \frac{Q_{\Delta t}}{V\cdot \mathrm{e}} \quad (12)$$

where N_{ion}: generation rate of negative ion [1/(s · m³)], $Q_{\Delta t}$: amount of charge generated per unit time [C/s], V: volume for the source of charge carrier [m³]. Figure 2b shows the profile of light intensity of DC-PD at the needle tip obtained from Figure 2a. In this paper, the standard deviation of light intensity profile in Figure 2b was defined as DC-PD equivalent diameter (2r = 1.55 mm), i.e. $V = 4/3 \cdot \pi \cdot r^3 = 1.95\times 10^{-9}$ m³ was applied.

$Q_{\Delta t}$ was calculated from the number of DC-PD current pulses and the amount of charge with the following equation:

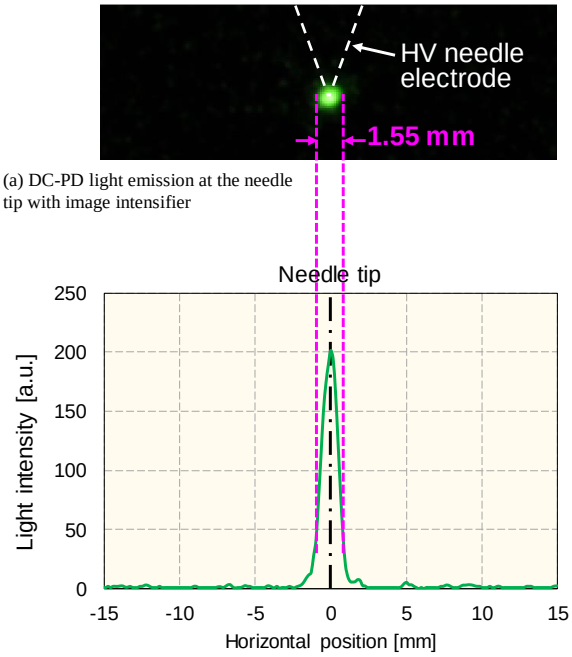

(a) DC-PD light emission at the needle tip with image intensifier

(b) Profile of light intensity for DC-PD at the needle tip

Figure 2. Light emission and light intensity of negative DC-PD (DC -10 kV, gap length 30 mm).

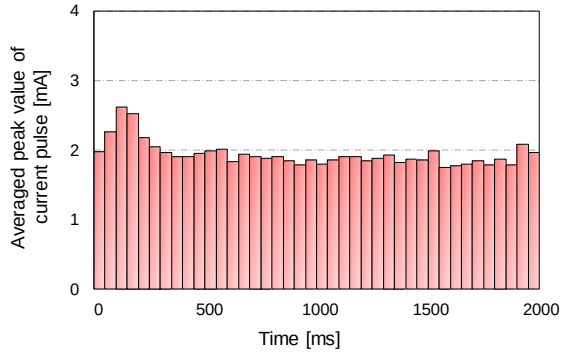

Figure 3. Time transition of averaged peak value of DC-PD current pulse (DC -10 kV, gap length 30 mm).

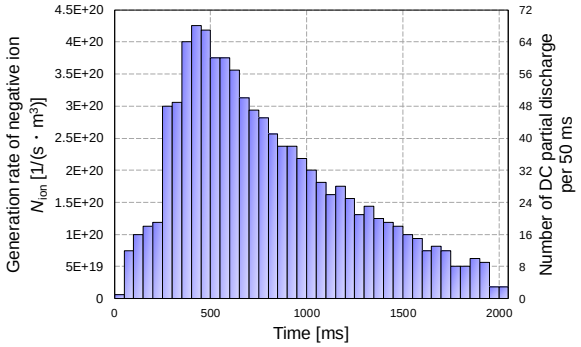

Figure 4. Time transition of number of DC-PD and generation rate of negative ion (DC -10 kV, gap length 30 mm).

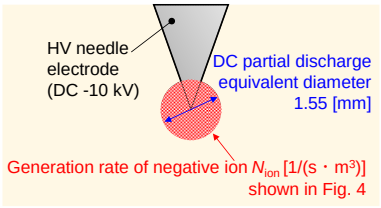

Figure 5. FEM simulation condition for DC-PD equivalent diameter and generation rate of negative ion at needle tip.

$$Q_{\Delta t} = n_{\mathrm{DCPD}} \cdot q_{\mathrm{C}} \quad (13)$$

where n_{DCPD}: number of DC-PD pulses per unit time [1/s], q_{C}: amount of charge per DC-PD current pulse [C]. Figure 3 shows the experimental result of the averaged peak value of PD current pulses per 50 ms from 0 to 2 s. Since the averaged peak value was approximately constant at 1.9 mA during the time transition, the amount of charge of q_{C} = 100 pC in consideration of pulse width was applied as a constant value. The blue bar charts in Figure 4 show the experimental result of the number of DC-PD per 50 ms from 0 to 2 s. As a result, the generation rate of negative ion N_{ion} was calculated by substituting (13) to (12). Figure 5 summarizes the DC-PD equivalent diameter and generation rate of negative ion at the needle tip in this simulation model. Assuming that the contour of the light emission in Figure 2a represents the PD extension limit, the generation rate of negative ion N_{ion} in Figure 4 was applied within the boundary of DC-PD equivalent diameter. By introducing the charge supply area around the needle tip, a novel simulation model considering the source of charge carrier due to DC-PD has been built.

3 RESULTS AND DISCUSSION

3.1 TIME TRANSITION OF CONDUCTIVITY DISTRIBUTION IN AIR

First of all, Figures 6a, 6b and 6c show the conductivity in air and equi-potential line distributions in steps of 5% (-0.5 kV per line gap) at 0.2 s, 0.6 s and 1 s after DC-on (0 s), respectively. The activated conductivity area in air is distributed between the HV needle electrode and PMMA by DC-PD generation at the needle tip. As one example, the activated conductivity in air at Point A is 6.50×10^{-9} S/m (0.2 s), 1.53×10^{-8} S/m (0.6 s) and 1.39×10^{-8} S/m (1 s), while the non-activated conductivity at Point B is 3.14×10^{-19} S/m (0.2 s), 2.87×10^{-19} S/m (0.6 s) and 3.50×10^{-19} S/m (1 s). The conductivity in air at Point A is approximately 10^{10} times higher than that at Point B. This is because the conductivity in air at Point A depends on the DC-PD at the needle tip, while the conductivity at Point B depends on the natural ionization as the main source of charge carriers. In the process of time transition, the electric field in air at the needle electrode tip is relaxed and the stress in PMMA is concentrated. This is because the negative charges generated by DC-PD at the needle electrode tip in Figure 2a are accumulated on PMMA surface.

3.2 COMPARISON WITH MEASUREMENT AND SIMULATION

Next, Figures 7a, 7b and 7c show the comparison of measured and calculated surface potential distributions on PMMA at each time. The plots show the average of the measured values, and the error bar shows the standard deviation. The number of measured data is 5 to 20. The negative potential emerged due to the negative charges accumulated on PMMA surface with a bell-shaped potential distribution. At Point C on PMMA below the needle tip, the surface potential was -1.2 kV (0.2 s), -2.5 kV (0.6 s) and -3.0 kV (1 s), resulting in the electric field concentration in PMMA and distortion as shown in Figures 6a, 6b and 6c. The activated conductivity area extended from the needle tip toward the PMMA edge due to the distortion of electric field distribution by the accumulated charges during time transition. This means that because the drift direction of charge in air is changed by the distortion of electric field distribution, the time evolution of surface potential distribution corresponds to the development of conductivity distribution in air toward PMMA edge. These charge behaviors are explained in the next section. Both measured and calculated surface potential distributions show good agreement.

Finally, Figure 8 shows the time transition of surface potential at Points C and D on PMMA, respectively. The value of surface potential is saturated in approximately 2 s. This is because DC-PD activities were suppressed, as shown in Figure 4, by the relaxation of electric field stress in air at the needle tip due to charge accumulation on solid insulator, in addition to the deflection of charge drift as explained in the next section. The time transition of calculated surface

potential shows the similar characteristics as the measured values.

3.3 EXTENTION OF ACTIVATED CONDUCTIVITY AREA DUE TO DISTORTION OF DRIFT DIRECTION

Figures 9a and 9b show the time transition of conductivity in air and the surface charge density distributions along PMMA surface from Point C to PMMA edge. The surface charge density distribution on PMMA extends in the

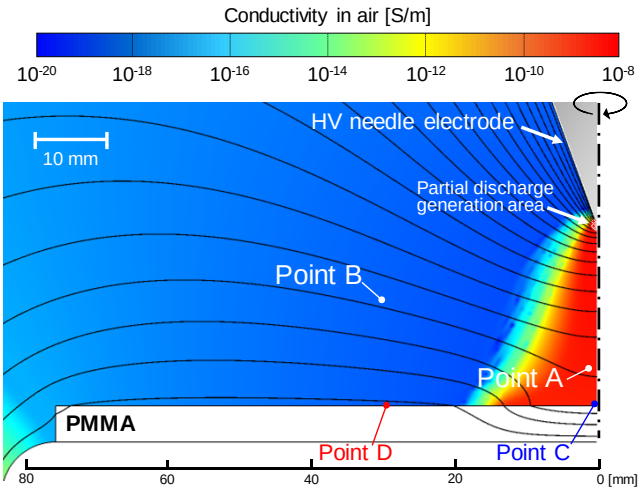

(a) At 0.2 s after DC-on

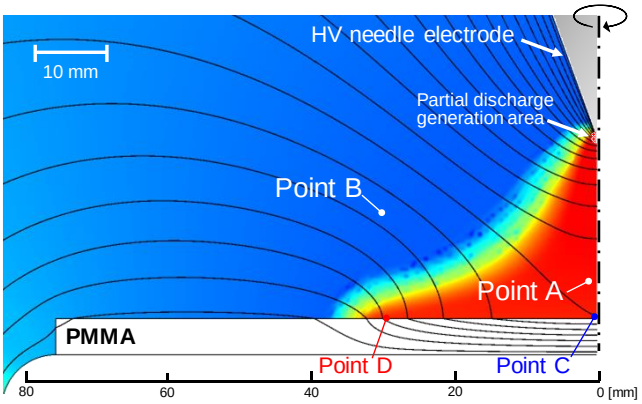

(b) At 0.6 s after DC-on

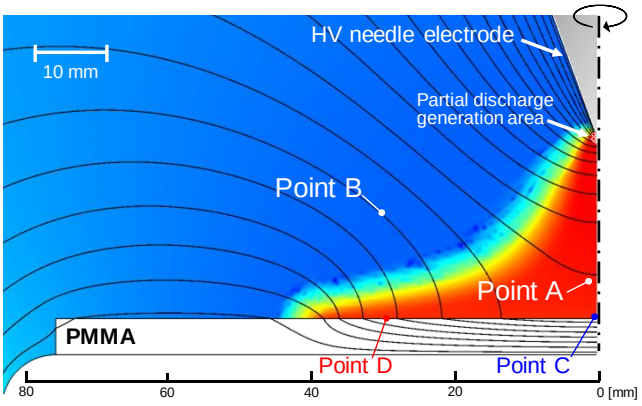

(b) At 1 s after DC-on

Figure 6. Conductivity in air and 5% equi-potential line distributions at each time in air-solid composite insulation systems (DC -10 kV, gap length 30 mm).

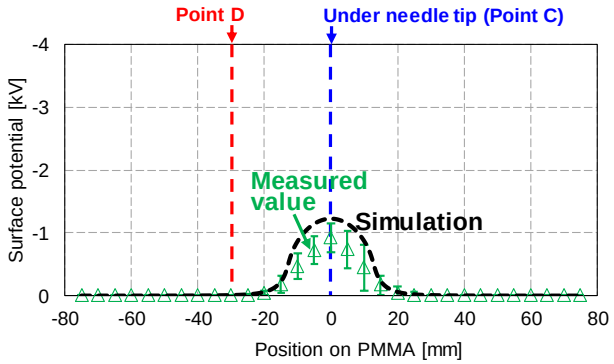

(a) At 0.2 s after DC-on

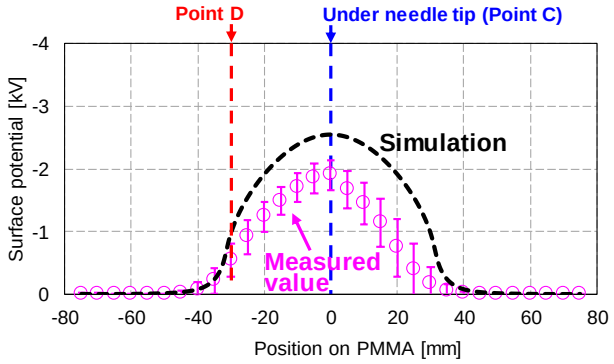

(b) At 0.6 s after DC-on

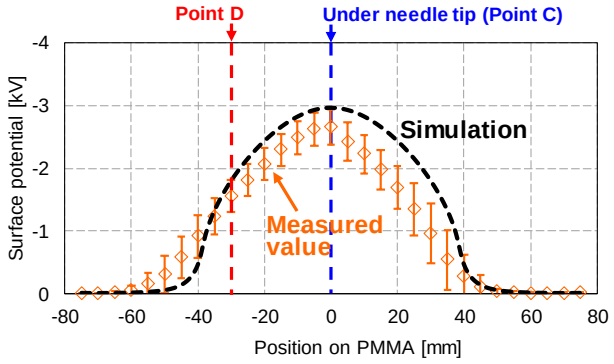

(c) At 1 s after DC-on

Figure 7. Surface potential distributions on PMMA at each time (DC -10 kV, gap length 30 mm).

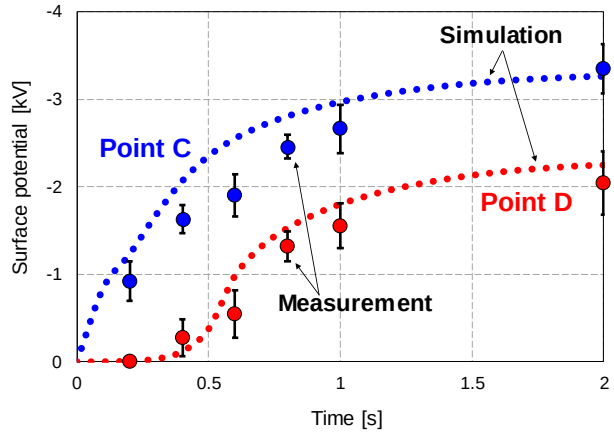

Figure 8. Time transition of surface potential on PMMA at each Point C and D from DC-on to DC steady-state.

direction of PMMA edge with the time transition of activated conductivity area in air. The activated conductivity in air contributing to the charge accumulation on PMMA surface was distributed in the range from 1.0×10^{-9} to 3.0×10^{-9} S/m.

Figure 9c shows the time transition of rate of increase for accumulated charge density distribution along PMMA surface at each time. The rate of increase for accumulated charge density distributions has the peak value at the edge of activated conductivity area in air at each time and the location of peak value transits in the direction of PMMA edge. In other words, the location where negative ions are mainly accumulated could transit in the radial direction during the time transition from DC-on to DC steady-state.

Figure 10 shows the schematic illustration of charging on solid insulator and distortion of drift direction under DC-PD in air-solid composite insulation systems, as explained above. At DC-on, the location where negative ions are mainly accumulated is just below the needle tip on PMMA (Figure 10a, red-colored ions). The drift direction of negative ions from the needle tip is deflected by the electric field distortion due to the charge accumulation on PMMA (Figure 10b, green-colored ions). As a result, the activated conductivity area in air is extended toward PMMA edge (Figure 10c, blue-colored ions). This means that the charge accumulation characteristics on solid insulator are determined by the time transition of activated conductivity area in air under DC-PD, until PD as the main source of charge carrier is entirely suppressed by the electric field relaxation at the needle tip under DC steady-state (Figure 10d).

As a result, we succeeded to estimate the activated conductivity distribution in air by DC-PD and clarified the charging process on solid insulator under negative DC voltage quantitatively. It was revealed that the time transition of charge accumulation on solid insulator corresponded to the distortion of activated conductivity area in air from DC-on to DC steady-state. The activated conductivity distribution in air is the dominant parameter that determines the charge accumulation process in air-solid composite insulation under DC-PD.

4 CONCLUSIONS

The investigation of the charging process on solid insulator under negative DC-PD was conducted in terms of the activated conductivity area in air by using needle-air-

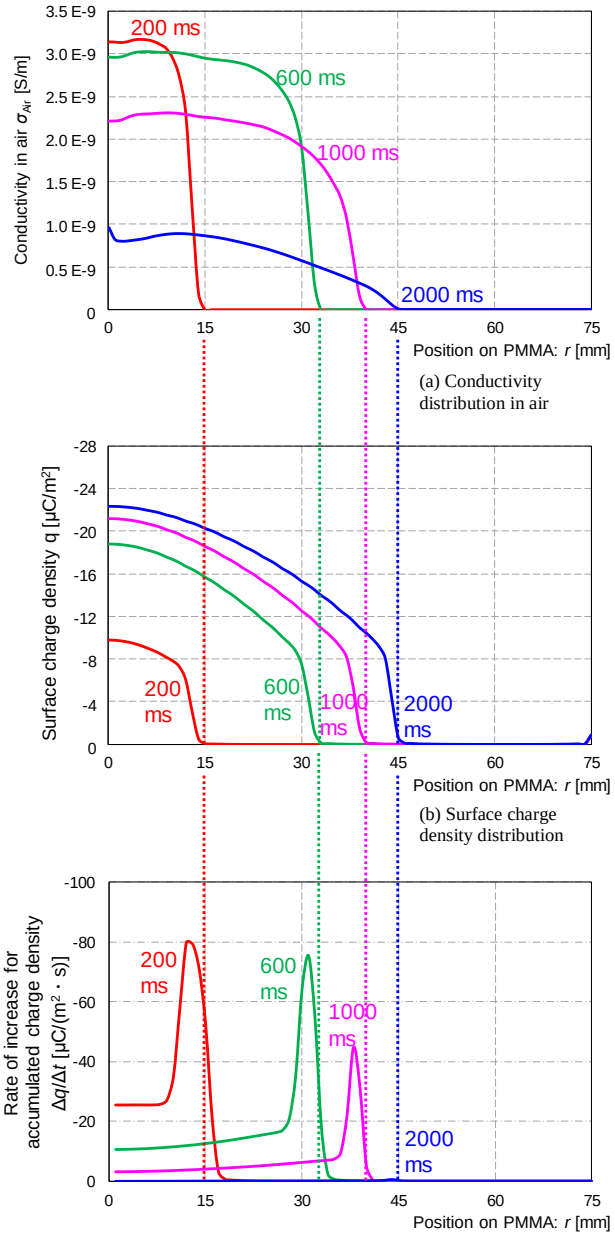

Figure 9. Transition of conductivity in air, surface charge density and rate of increase for accumulated charge density distributions along PMMA surface at each time (DC -10 kV, gap length 30 mm).

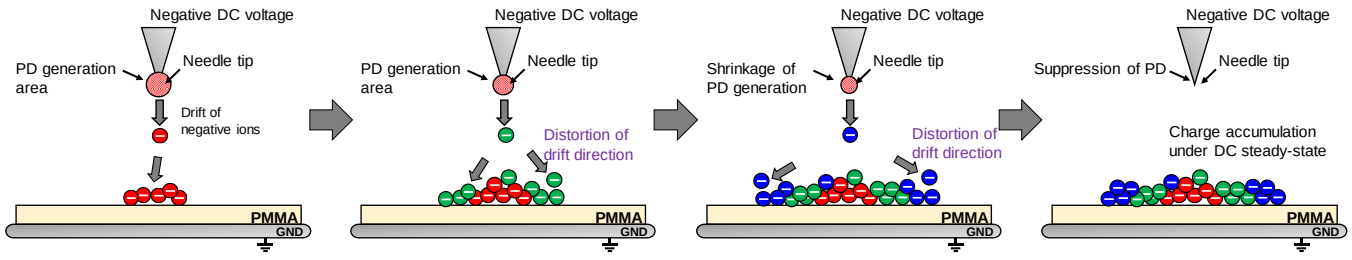

Figure 10. Schematic illustration of charging on solid insulator and distortion of drift direction mechanism under DC-PD in air-solid composite insulation systems.

PMMA-plane electrode configuration with air gap 25 mm under negative DC 10 kV application. Measured surface potential on solid insulator was compared with the calculated value considering charge activities in air. Especially, a novel transport equation model was built considering the source of charge carrier generation by DC-PD based on experimental data such as the shape and frequency of DC-PD. The followings were concluded:

1. The activated conductivity area was distributed in air and extends from the needle tip toward the PMMA edge from DC-on to DC steady-state. This is because the electric field distribution is distorted by the emergence of surface potential on PMMA due to the negative charges accumulated and the drift direction of charge in air is changed.

2. The surface potential on PMMA was saturated in approximately 2 s. This means that DC-PD activities at the needle tip are suppressed by the charge accumulation in addition to the deflection of charge drift. Both measured and calculated surface potential distributions and their time transition characteristics show good agreement.

3. The surface charge density distribution on PMMA extended with the time transition of activated conductivity area in air. The location where negative ions are mainly accumulated could transit in the radial direction, until DC-PD as the main source of charge carrier is entirely suppressed by the electric field relaxation by charge accumulation on PMMA.

4. The activated conductivity in air contributing to the charge accumulation on PMMA surface was distributed in the range from 1.0×10^{-9} to 3.0×10^{-9} S/m under DC-PD, which is approximately 10^{10} times higher than that in non-activated conductivity space by natural ionization.

As a result, we quantitatively clarified the processes that DC-PD as the source of charge carrier contributes to the charge accumulation in terms of the activated conductivity distribution in air. This means that the activated conductivity distribution in air is the dominant parameter that determines the charge accumulation process in case that charge behavior is activated in gas medium under DC-PD from DC-on to DC steady-state.

REFERENCES

[1] O. Kuhn *et al*, "2nd generation DC grid access for offshore wind farms: HVDC in an AC fashion," Cigre Session 46, B3-110, 2016.

[2] T. Yasuoka *et al*, "Insulation characteristics in DC-GIS: Surface charge phenomena on epoxy spacer and metallic particle motions,, Cigre Session 47, D1-103, 2018.

[3] H. Fujinami, T. Takuma, M. Yashima, and T. Kawamoto, "Mechanism and effect of DC charge accumulation on SF_6 gas insulated spacers," IEEE Trans. Pwr. Del., vol. 4, No. 3, pp. 1765-1772, 1989.

[4] R. Nakane, K. Takabayashi, K. Kato, and H. Okubo, "Electrical insulation performance of HVDC-GIS spacer under various testing conditions," *Annu. Rep. IEEE Conf. Electr. Insul. Dielectr. Phenom.*, pp.621-624, 2017.

[5] H. Iwabuchi *et al*, "Influence of tiny metal particles on charge accumulation phenomena of GIS model spacer in high-pressure SF_6 gas," IEEE Trans. Dielectr. Electr. Insul. Vol. 20, No. 5, pp. 1895-1901, 2013.

[6] H. Okubo, R. Nakane, and K. Okamoto, "Partial discharge inception characteristics in air with solid dielectrics under HVDC and polarity Reversal Conditions," *Annu. Rep. IEEE Conf. Electr. Insul. Dielectr. Phenom.*, 2018, pp.481-485.

[7] M. Tschentscher and C. M. Franck, "Conduction processes in gas-insulated HVDC equipment: from saturated ion currents to micro-discharge," IEEE Trans. Dielectr. Electr. Insul, Vol. 25, No. 4, pp. 1167-1176, 2018.

[8] A. Winter and J. Kindersberger, "Stationary resistive field distribution along epoxy resin insulators in air under DC voltage," IEEE Trans. Dielectr. Electr. Insul., Vol. 19, No. 5, pp. 1732-1739, 2012.

[9] C. Cooke *et al*, "Polarization and charge transport in unfilled epoxy," *IEEE Int. Symp. Electr. Insul. Materials (ISEIM)*, 2005, Vol. 1, pp. 69-72.

[10] J. Kindersberge and, C. Lederle, "Surface charge decay on insulators in air and sulfurhexafluorid-Part I: simulation," IEEE Trans. Dielectr. Electr. Insul., Vol. 15, No. 4, pp. 941-948, 2008.

[11] K. Nakanishi, A. Yoshioka, Y. Arahata, and Y. Shibuya, "Surface charging on epoxy spacer at DC stress in compressed SF_6 gas," IEEE Trans. Pwr. Del., vol. PAS-102, No. 12, pp. 3919-3927, 1983.

[12] M. Schueller, U. Straumann, and C. M. Franck, "Role of ion sources for spacer charging in SF_6 gas insulated HVDC systems," IEEE Trans. Dielectr. Electr. Insul., vol. 21, no. 1, pp. 352-359, 2014.

[13] T. Vu-cong *et al*, "Surface charge measurements on epoxy spacer in HVDC GIS/GIL in SF_6," *Annu. Rep. IEEE Conf. Electr. Insul. Dielectr. Phenom. (CEIDP)*, 2016, pp. 93-96.

[14] R. Gremaud *et al*, "Solid-gas insulation in HVDC gas-insulated systems: measurement, modeling and experimental validation for reliable operation," Cigre Session 49, D1-101, 2016.

[15] A. Winter and J. Kindersberger, "Transient field distribution in gas-solid insulation systems under DC voltages," IEEE Trans. Dielectr. Electr. Insul., vol. 21, No. 1, pp. 116-128, 2014.

[16] T. Yasuoka *et al*, "Numerical simulation of electrical conduction phenomena in various insulating gases (SF_6, Dry Air, CO_2 and N_2)," *IEE Japan annu. meeting*, 2014, no. 6-279.

[17] N. Lavesson and C. Doiron, "Hybrid resistive-capacitive and ion drift model for solid gas dielectrics," 2015 Comsol Conference, 2015.

Ryuichi Nakane (M'18) was born in Gifu, Japan in 1994. He received a M.S. degree in electrical engineering from Aichi Institute of Technology, Japan in 2019. He is currently a Ph.D. candidate of Nagoya University, Japan. He is a student member of IEE of Japan.

Hiroki Kojima (M'11) was born on December 7, 1975. He received a Ph.D. degree in 2004 in energy engineering and science from Nagoya University. He has been at Nagoya University since 2004, where he is presently at Associate Professor in the Department of Electrical Engineering. Dr. Kojima is a senior member of IEE of Japan.

Naoki Hayakawa (M'90) was born on September 9, 1962. He received a Ph.D. degree in 1991 in electrical engineering from Nagoya University. He has been at Nagoya University since 1990, where he is presently a Professor in the Department of Electrical Engineering. From 2001 to 2002, he was a guest scientist at the Forschungszentrum Karlsruhe, Germany. Prof. Hayakawa is a member of IEE of Japan and CIGRE.